Characterization of Spongelike Porous Polyvinylidene Fluoride (PVDF) for use as a Biosensor

A Thesis

SUBMITTED TO THE FACULTY OF THE UNIVERSITY OF MINNESOTA-DULUTH

BY

Matthew Danley

IN PARTIAL FULFILLMENT OF THE REQUIREMENTS

FOR THE DEGREE OF

MASTER OF SCIENCE

Advisor:

Victor K. Lai, Ph.D.

Committee Members:

Melissa Maurer-Jones, Ph.D.

Ping Zhao, Ph.D.

August 2021

Acknowledgments

I would like to thank my advisor, Dr. Victor Lai, of the Chemical Engineering department at the University of Minnesota-Duluth. He was always available for questions regarding research, homework, and guidance on my academic career.

I would also like to thank my committee members Dr. Maurer-Jones and Dr. Ping Zhao. They both provided training and support on instrumentation essential to this project. Without their help, I would not have been able to finish this degree.

I would like to thank the other Chemistry master's degree students, Janna Quick and Chioma Nwachuku. They kept me on track regarding coursework and always provided positive encouragement when having instrumentation issues.

I would like to thank my fellow research group members, Steven (Zhaolin) Gao, Jack Kloster, and Jared Tucker for their work and support on this project. Without them, I would not have been able to finish this project. I would like to thank other group members for their ongoing support in Dr. Lai's research group, Chris Vidmar, Katelyn France, and Sonia Li. You all made being a part of this research group an enjoyable experience!

Finally, I would like to thank Lyndon Ramrattan for his help as the Chemical Engineering Lab Services Coordinator. I am thankful for Lyndon always being willing to help fix any issues I had with lab materials!

Abstract

The Transcatheter Aortic Valve Replacement (TAVR) is a minimally invasive procedure that has grown in popularity in recent years, by using a catheter to deploy a replacement valve in patients with heart valve stenosis. Although minimally invasive, there are document complications, including a morality rate of 8.4% for TAVR procedures compared to 4.8% for tissue surgery procedures after 90 days for Medicare beneficiaries. It is proposed that the replacement valve alters blood flow and blood pressure after implantation and causes the complications. Instead of studying the changes in a living patient, creating a 3D printed model of the aortic tissue and studying the effects in-vitro is ideal, with a biosensor needed to detect these changes in blood flow and blood pressure. Polyvinylidene Fluoride (PVDF) is a piezoelectric polymer that is a promising material for the biosensor by generating different voltages in response to mechanical stresses such as compression forces. Porous PVDF samples have shown higher piezoelectric properties compared to nonporous membranes. It is thought that the increase in porosity allows the polymer chains to flex more and generate a larger piezoelectric output. Removing too much PVDF, however, negates any advantage of inducing pores, so there is an optimal porosity that will give the maximum piezoelectric output. The goal of this study is to find the optimal porosity of PVDF samples for use as a biosensor. By adding Zinc Oxide (ZnO) in various amounts to a solution of PVDF and 2-butanone during the fabrication process, and subsequently removing via an HCl acid bath once the 2-butanone was evaporated, porous PVDF sensors were made. The porosity of the PVDF samples were found using the gravimetric method. Fourier Transform Infrared (FTIR) spectroscopy was used to study the different polymer chain conformations, and to quantify the amount of piezoelectric chains in the PVDF sensors. There are three main chain conformations in PVDF, an α phase, β phase and γ phase. The β phase and γ phases are desired since they exhibit piezoelectric properties. The piezoelectric output of the PVDF sensors was quantified by calculating the d_{33} piezoelectric coefficient. By collecting the voltage generated from the sensors under different compressive loads. Results showed that the addition of ZnO nanoparticles to the PVDF sensors altered the porosity of the samples. As the amount of ZnO was increased during the fabrication process, the porosity of the PVDF sensors increased, which was expected. Changes in the amount of ZnO added during the fabrication process also led to statistically significant differences in the amount of piezoelectric chain conformations, but no trend or pattern with ZnO amount was observed. A trend emerged in which the piezoelectric properties increased as the amount of ZnO used during fabrication increased up to 30%wt ZnO, and then the piezoelectric output decreased at 40% and 50%wt ZnO, which is supported by literature. The d_{33} coefficient at 30%wt ZnO was found to be 1.8pC/N. Overall, the d_{33} coefficients increased as the amount of piezoelectric chain conformations increased in the sensors. This shows that the d_{33} values are dependent on the amount of piezoelectric chain conformations along with porosity. In summary, altering the amount of ZnO nanoparticles during the fabrication process led to changes in

porosity and the amounts of piezoelectric chain conformations. Both factors affected the piezoelectric output of the sensors. Going forward, the fabrication process needs to be modified to control the amounts of piezoelectric chain conformations present in the PVDF samples which should increase the piezoelectric properties of the sensors.

Table of Contents

List of Figures

List of Abbreviations

Abbreviations	Description
PVDF	Polyvinylidene Fluoride
TAVR	Transcatheter Aortic Valve Replacement
MB	Medicare Beneficiaries
SAVR	Surgical Aortic Valve Replacement
DMSO	Dimethyl sulfoxide
ZnO	Zinc Oxide
FTIR	Fourier Transform Infrared Spectroscopy
wt%	Weight percent
PZT	Lead Zirconate Titanate

Chapter 1. Introduction

1.1 Transcatheter Aortic Valve Replacement (TAVR) Procedure

The TAVR is a minimally invasive procedure that uses a catheter to deploy a replacement valve for patients with various degrees of heart valve stenosis [1]. Heart valve stenosis is the diseased state of a heart valve that reduces the amount of blood flow due to damage from calcium or scarring [2]. Figure 1 shows an example of valve stenosis as well as how the catheter deploys the replacement in the aortic tissue. Since it is minimally invasive, some Medicare beneficiaries (MB) undergo TAVR when they are deemed ineligible for a surgical procedure [3]

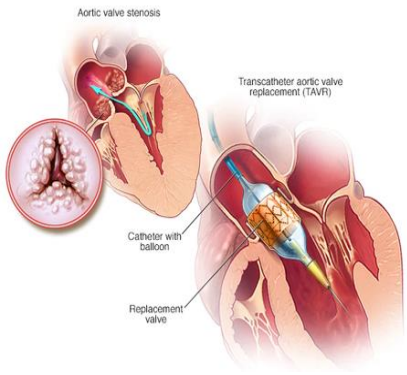

Figure 1. Heart valve stenosis and deployment of replacement valve[2]

For patients that cannot undergo open-heart surgery, the TAVR procedure gives hope for survival since in the past surgical aortic valve replacement (SAVR) was the only option [4]. Since TAVR is minimally invasive, some patients are able to walk around right after the procedure and can be discharged within a few days [4]. It is noted that MB undergoing TAVR procedures had fewer adverse events (which included new-onset hemodialysis, transfusion, vascular complications, infections, strokes, congestive heart failure, postoperative adult respiratory distress syndrome, acute renal failure, or implanted pacemakers) than MB undergoing other aortic valve procedures [3]. Since the TAVR and SAVR procedures have had similar results with high-risk and intermediate patients, one question going forward is if the TAVR will have similar results in a low-risk population [3].

Even though TAVR has many benefits, there are documented complications for the procedure. From 2012-2015, the in-hospital mortality rates, cumulative 30-day mortality rates, and 90-day post-discharge mortality rates declined annually for both TAVR and SAVR, but the 90-day mortality rate for TAVR was nearly double the rate for SAVR procedures [3]. Further studies found that between 2012 and 2017 11% of patients

undergoing a TAVR procedure had a pacemaker implanted during the same hospitalization period, and 1.1% of patients had a pacemaker implanted during a subsequent hospitalization after the TAVR procedure [5]. 79.6% of these pacemakers implanted due to the TAVR procedure were implanted within 14 days of TAVR surgery [5]. These studies and statistics about all these complications of the TAVR compared to SAVR are concerning and warrant further study.

Unfortunately, there is no consensus on why these problems arise despite the many documented cases of complications post TAVR procedure. One hypothesis is that introducing a mechanical valve into diseased heart tissue could alter the microenvironment and change the flow and pressure of blood, but studying these changes in a living patient could be difficult. Patients could be monitored for any changes in heart rate and blood flow in the hospital, but implanting sensors into patients that are not fit for open-heart surgery does not seem ideal or ethical and seems counterintuitive to the TAVR procedure. Rather, studying how the replacement valve affects the surrounding heart tissue should be done in-vitro to reduce the possibility of complications in a living patient.

One way to investigate the complications from the TAVR procedure in-vitro is to create a model aortic tissue sample that mimics human tissue. Other groups have shown that it is possible to 3D print an aortic tissue sample for use in biomedical studies [6–8]. For example, one group 3D printed an aortic model using polylactic acid polymers, PLA 4043D (Natureworks LLC) and Filaflex (Recreus, Spain), to look at a bicuspid aortic valve [6]. Although this model was flexible and had the correct structure of the aortic valve, not all properties were similar to human tissue [6]. Using silicone that mimics human heart tissue to make the aortic heart tissue would allow studies in-vitro since the environment would be the same as a human heart. Therefore, the overall goal of this project is to design a working model to understand what occurs before and after the implantation of the replacement valve. Specifically, this study will look at creating and characterizing a small biosensor that will track changes in blood flow and pressure in a silicone heart model. This sensor will need to be small and sensitive to small changes in pressure. One promising material is Polyvinylidene Fluoride (PVDF) since it is a piezoelectric polymer

that has properties that are beneficial for use as a biosensor. Using a piezoelectric material is ideal since other studies have shown that piezoelectric materials can be used as a sensor [9–12].

1.2 Polyvinylidene Fluoride (PVDF): Structure and Properties

PVDF, also known as 1,1-difluoriethylene, is a polymer that is comprised of fluorine and hydrogen atoms along a carbon backbone. Different arrangements of the fluorine atoms and hydrogen atoms allow for the polymer to become polarized due to the differences in electronegativities, and therefore exhibit piezoelectric properties.

PVDF can form five different crystalline polymorphs, or chain conformations, which are denoted as *α, β, γ, δ, and ε* [13–15]. Specifically, the *α, β, γ* chain conformations are of interest, since those are common chain conformations present in the PVDF. Figure 2 shows the different chain conformations of *α, β, γ* orientations. The *β* chain conformation has been shown to have the highest piezoelectric properties since the orientation of the carbon backbone bonds are all trans orientation which leads to a high polarization [13,14]. The *γ* chain conformation has some piezoelectric properties but not as large as a *β* chain conformation due to a gauche orientation every 4th bond in the chain [13,14]. The *α* chain conformation has not shown any piezoelectric properties since it does not become polarized due to alternating trans and gauche bonds [13]. This means a good PVDF piezoelectric sensor would have high *β and γ* chain conformations present and lower concentrations of α chain conformations.

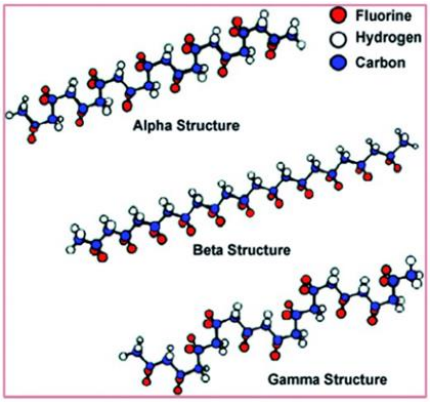

Figure 2. Different chain conformations of PVDF[10].

Piezoelectric materials generate an electrical charge in response to a mechanical stress. Specifically, a piezoelectric sensor would generate a measurable voltage in response to a change in applied mechanical forces. This type of material would be useful since any changes in pressure or flow rates would be calibrated to changes in voltage which can be measured. An ideal material for a sensor would have a high piezoelectric coefficient, which is used to quantify the piezoelectric output for a given material. Piezoelectric coefficients are reported as d_{31}, d_{32}, and d_{33} values, which show the orientation of the mechanical changes and the location of the generation of electricity. In piezoelectricity, the *X-Y-Z* planes are denoted as *1-2-3*, with the first number in the piezoelectric coefficient denoting the direction of the mechanical force applied and the second number showing the orientation of the generation of electricity. Figure 3 shows the orientations of *1,2* and *3* mapped to an *X, Y, Z* orientation. Since the sensor needed for the study of complications from the TAVR procedure needs to detect changes in blood flow and blood pressure, the material would need a high piezoelectric coefficient with the mechanical stress and electricity generations in the same plane, since the samples would be compressed under different blood pressures. This means the ideal material should have a high d_{33} coefficient.

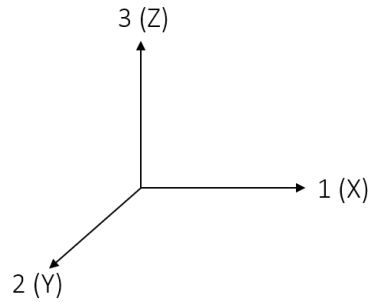

Figure 3. X Y Z and 1 2 3 denotations of piezoelectric coefficients

PVDF has been used as a biosensor in the past, e.g. to measure the heart rate and calculate the velocity of a pulse on a human [16–18]. Even though these studies show that PVDF can be used as a biosensor, one study used a very large PVDF sample, 152cm^2 and 15mm high, which would be too large to fit in a model aortic heart valve without disrupting blood flow [16]. Another study had to amplify the signal measuring pulse [17]. This means a PVDF sensor would have to be modified to increase the piezoelectric signal from a given sample.

One method that has been shown to raise the piezoelectric properties of PVDF is to induce pores into the membrane [19,20]. It is thought that removing some PVDF would allow the present chains to deform more as they collapse into the pores, which would generate a larger piezoelectric output [19]. One study found that by casting PVDF with Dimethyl sulfoxide (DMSO), freezing the solution, and then removing the DMSO, that the remaining PVDF structure could generate a larger piezoelectric coefficient[20]. This specific method made samples that had "long lateral" pores [20] shown in Figure 4A. These samples that were about 1.5mm thick generated d_{33} coefficients up to 264pC/N [20]. Another study made porous PVDF films by adding and removing Zinc Oxide (ZnO) nanoparticles before and after casting [19]. This left behind a structure similar to a sponge, with small pores all around the sample [19] shown in Figure 4B. This study found that by inducing pores with various amounts of ZnO, the voltage generated changed [19]. However, Mao et al did not calculate the d_{33} coefficient.

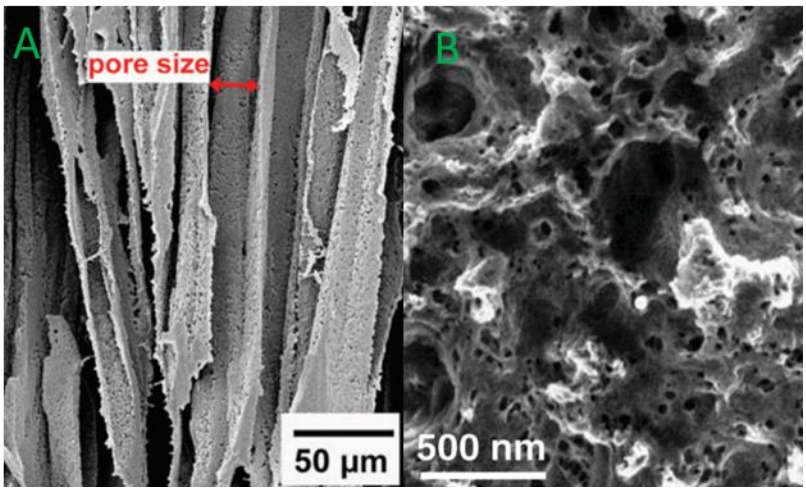

Figure 4. Porous PVDF Samples. Image A shows the scanning electron microscope image of an ice templated PVDF sample with lateral pores[12]. Image B shows a porous PVDF samples made from adding and removing ZnO nanoparticles during the fabrication process[11]

Hence, the overall objective of this study is to investigate how inducing pores into a spongelike PVDF membrane affects the d_{33} piezoelectric coefficient for use as a biosensor. These sensors will be mechanically characterized via compression using a tensile tester and structurally using Fourier Transform Infrared (FTIR) spectroscopy.

Chapter 2. Fabrication and Characterization of PVDF Sensors

2.1 Fabrication of Nanoporous PVDF Sensors

The spongelike porous PVDF sensors were fabricated similar to the protocol reported in [19]. PVDF powder (Alfa Aesar, Ward Hill, MA) was dissolved in 2-butanone solvent (Alfa Aesar, Ward Hill, MA) at 80°C. ZnO nanoparticles were added to the mixture (35-45nm, US Research Nanomaterials, Houston, TX), then the solution was placed in an ultrasonication bath for 30 minutes and vortexed to ensure a homogenous mixture. The amount of ZnO nanoparticles added to the PVDF solution was varied to create different wt% ZnO membranes. The solution was then poured into a 40mL glass petri dish and placed in an oven at 80°C. Once all the 2-butanone was evaporated from the PVDF/ZnO solid structure, the resulting membranes were placed in a 10M hydrochloric acid (Avantor Inc., Allentown, PA) for 24 hours to remove the ZnO and leaving the spongelike porous PVDF structure behind as shown in Figure 5.

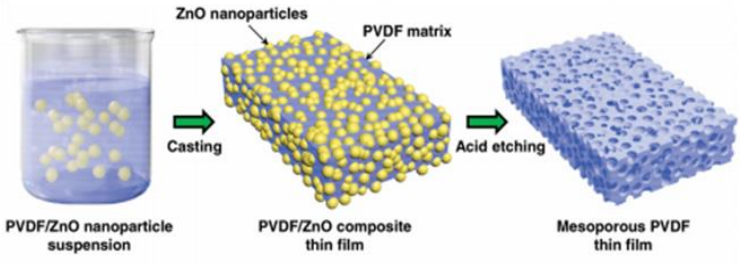

Figure 5. PVDF fabrication with ZnO nanoparticles[11]. The ZnO nanoparticles are added to a solution of PVDF dissolved in 2-butanone. This suspension is then cast into a petri dish and the 2-butanone is evaporated off leaving a PVDF/ZnO composite thin film. After being placed in an acid bath, a spongelike mesoporous PVDF thin film is left.

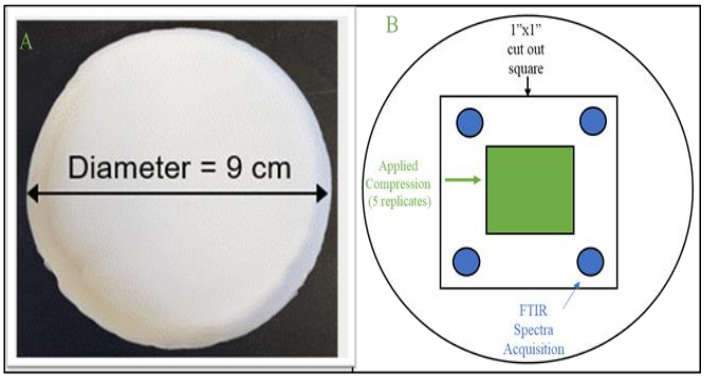

Figure 6. Fabricated PVDF sample. Image A shows a fabricated PVDF sensor. Image B shows where the compression force was applied and where the FTIR spectra was collected on the 1"x1" square.

A square of 1"x1" was cut from the circular membranes with ¾"x ¾" copper tape electrodes placed on either face of the sensors. ½" width copper tape leads were attached to the copper tape electrodes to allow for connection to a modified Sawyer-Tower circuit in mechanical testing. The copper tape electrodes and leads were placed on the PVDF

sensors in such a way to allow for mechanical testing in structural testing on the same sample. Figure 6A shows the dried PVDF sensor and Figure 6B shows where the compressions and FTIR spectra were collected.

Along with the fabricated sensors, PVDF samples from PolyK Technologies (State College, PA) were studied. These bought samples were used as a standard as a comparison to the structural and mechanical properties of the fabricated PVDF sensors.

2.2 Porosity of PVDF Films

One method to characterize the structure of the PVDF sensors is to calculate the porosity or the volume percent of empty space within the sensor. This can be done by using the gravimetric method outlined by Roshani et al.[21] To calculate the percent porosity, the square PVDF sensors were weighed before being placed in a methanol bath for 30 minutes ($m_{initial}$). After soaking, the PVDF sensors were removed from the bath and a Kim wipe was used to remove any excess methanol and then promptly weighed again (m_{final}). The change in mass after the bath is due to the methanol that is trapped inside the pores of the PVDF sensor. Using the following equation, the percent porosity of the PVDF sensors can be calculated:

$$\%\ Porosity = \frac{(m_{final} - m_{intial}) * \rho_{PVDF}}{\rho_{PVDF} * m_{final} + (\rho_{Methanol} - \rho_{PVDF}) * m_{initial}} \quad (1)$$

Where ρ_{PVDF} is the density of PVDF (1.78g/cm^3), and, $\rho_{Methanol}$is the density of methanol (0.792g/cm^3). This equation simplifies to calculating fraction volume of methanol compared to the total volume of the sensor and methanol.

2.3 Chain Conformation and Crystallinity of PVDF Films

Characterizing the crystalline structure and quantifying the amount of piezoelectric chain conformations present was done using FTIR Spectroscopy. It has been documented that the different chain conformations have different FTIR spectra from each other which allows for calculating the relative amounts of each chain conformation [13,14,22–24]. This is due to the different crystal structures and the changes in the carbon chain backbone of the polymer. For example, vibrational bands at 530cm^{-1}, 615cm^{-1}, 765cm$^{-1,}$ and 795cm^{-1} refer to the α phase of PVDF due to CF_2 bending, skeletal bending and CH_2

rocking and bands at 510cm^{-1} and 840cm^{-1} are due to CF_2 bending and CH_2 rocking in the β phase[22–24]. Bands at 1234cm^{-1} are due to CF out of plane deformation and this is unique to the γ phase of PVDF[24]. The CF_2 bending, skeletal bending, and CH_2 rocking are due to the different arrangement of the bonds in the polymer. For β phase chains, the bonds are all trans for the carbon backbone. The α phase alternates between trans and gauche bonds for the carbon backbone. γ phase of PVDF has three trans bonds and then one gauche bond which repeats in sets of four. This means that some bond angles of the carbon atoms are different depending on the phase conformation present. These different vibrations of the polymer chain can be identified by an FTIR and used to calculate the relative amounts of α phase and $\beta+\gamma$ phases. The $\beta+\gamma$ phases will be calculated together since both have some piezoelectric properties.

A Nicolet iS50 FT-IR (Thermo Scientific, Waltham, MA) instrument was controlled by Ominic software, which collected 64 scans for each spectrum at a resolution of 4cm^{-1}. Four replicates were collected on each sample, one at each corner of the square film next to the copper tape electrode, which is shown in Figure 6 and Figure 8. The analysis of each spectrum to obtain the fraction of each crystalline phase is detailed in Cai et al.[13] Figure 7 shows the whole FTIR spectra of the PVDF sensor. To quantify the amount of each chain conformation present in the sensor, the electroactive phases, or phases that exhibit piezoelectric properties are calculated first.

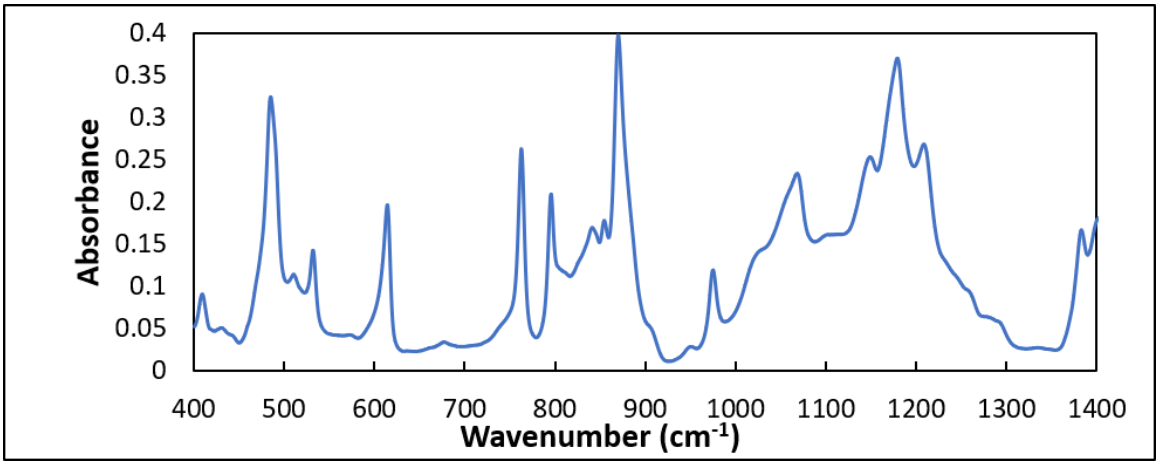

Figure 7. Whole FTIR Spectra of PVDF sensor.

Briefly, the fraction of electroactive conformations β and γ, F_{EA}, is calculated using equation 2:

$$F_{EA} = \frac{I_{840cm^{-1}}}{\left(\frac{K_{840cm^{-1}}}{K_{763cm^{-1}}}\right) * I_{763cm^{-1}} + I_{840cm^{-1}}} * 100\% \quad (2)$$

where I_{840} is the absorbance from the spectra at 840cm^{-1}, I_{763} is the absorbance from the spectra at 763cm^{-1}, K_{840} is the absorption coefficient at 840cm^{-1} which is 77,000 cm^2*mol^{-1} and K_{763} is the absorption coefficient at 763cm^{-1} which is 61,000cm^2*mol^{-1}. Figure 8 zooms in on the spectra in Figure 7 and shows where the absorbance values were taken from. This allowed for the calculation between fraction α comparing to fraction β and γ.

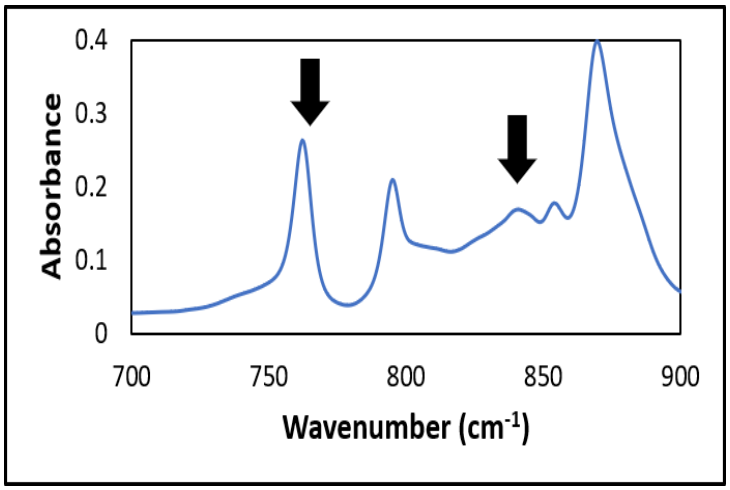

Figure 8. FTIR spectra for calculating the fraction of electroactive phases of PVDF. The black arrows show where the absorbance values were taken for calculations.

Subsequently, equations 3 and 4 are used to separate the amount of β *and* γ phases respectively:

$$F(\beta) = F_{EA} * \left(\frac{\Delta H_\beta}{\Delta H_\beta + \Delta H_\gamma}\right) * 100\% \quad (3)$$

$$F(\gamma) = F_{EA} * \left(\frac{\Delta H_\gamma}{\Delta H_\beta + \Delta H_\gamma}\right) * 100\% \quad (4)$$

where ΔH_β is the difference in absorbance values between the nearest peak at 1275cm^{-1} and the nearest valley at 1260cm^{-1}, and $\Delta H\gamma$ is the difference in absorbance values at the nearest peak at 1234cm^{-1} and the nearest valley near 1225cm^{-1}. Figure 9 shows the portion of the spectra used to calculate the individual values of β and γ. The amount of β and γ phases were calculated separately and then later combined.

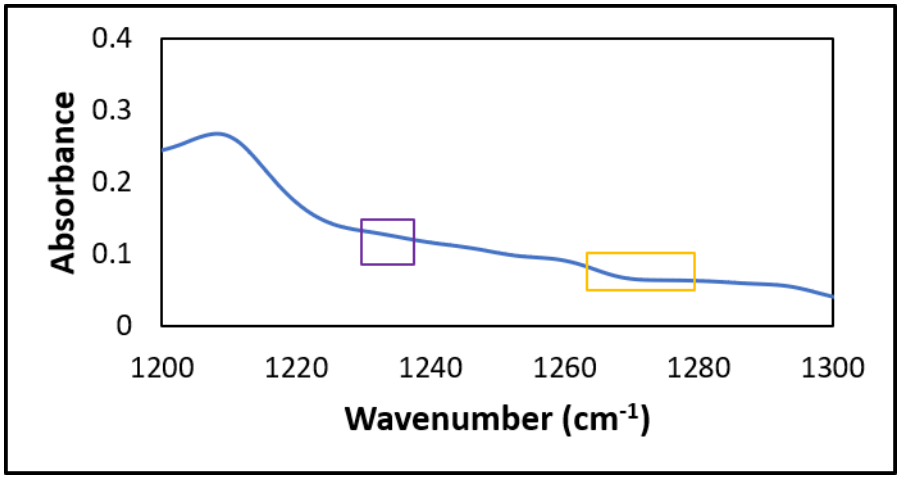

Figure 9. FTIR spectra for calculating the β and γ phases of PVDF. The yellow box shows the region of spectra for β phase chain conformation calculations outlined in equation 3. The purple box shows the region for γ phase calculations using equation 4.

2.4 Mechanical Characterization

There are many ways to find the d_{33} coefficient of piezoelectric materials, such as using a d_{33} meter [20] and using a pneumatic pressure rig [25]. It would be convenient and easy to use a d_{33} meter for characterizing PVDF, but it has been documented that d_{33} meters may not give the most accurate results on thin films or very thin samples[26 27] . Instead, the d_{33} coefficient is calculated by compressing the PVDF sensors using a tensile tester and measuring the voltage from that compression using a National Instruments cDAQ and LabView. To confirm this method of calculating the d_{33} coefficient works, the instrument was calibrated by testing lead zirconate titanate (PZT) ceramic standards. These PZT samples were tested on the d_{33} meter, which works for thicker samples, and then on the tensile tester. To calculate the d_{33} coefficient for spongelike porous PVDF, the sensors were subjected to displacement compression tests using a Test Resources Newton 100 series Tensile

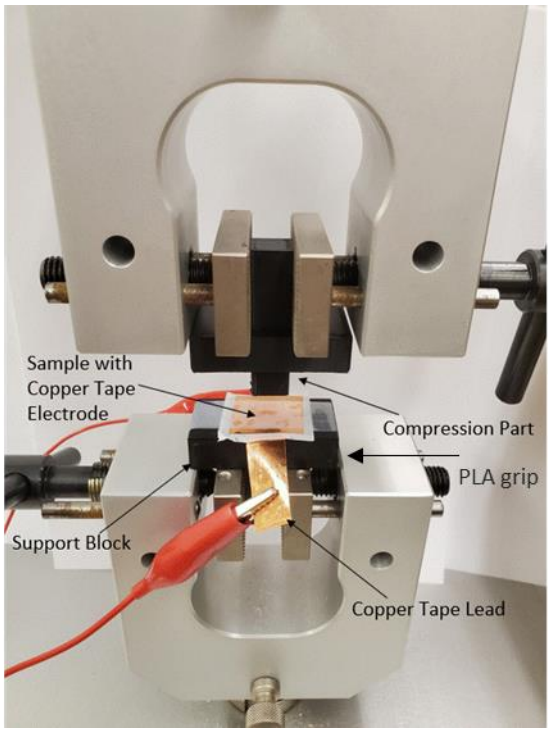

Figure 10. Set up for compression tests on PVDF sensor. The PVDF sample is taped down to the PLA grip and connected to the Modified Sawyer-Tower circuit via the copper tape leads.

Tester with a 1000lb$_f$ actuator (Test Resources Inc, Shakopee, MN), and voltage generated was collected on a National Instruments NI cDAQ-9174 chasses and NI 9215 input module controlled by LabView software.

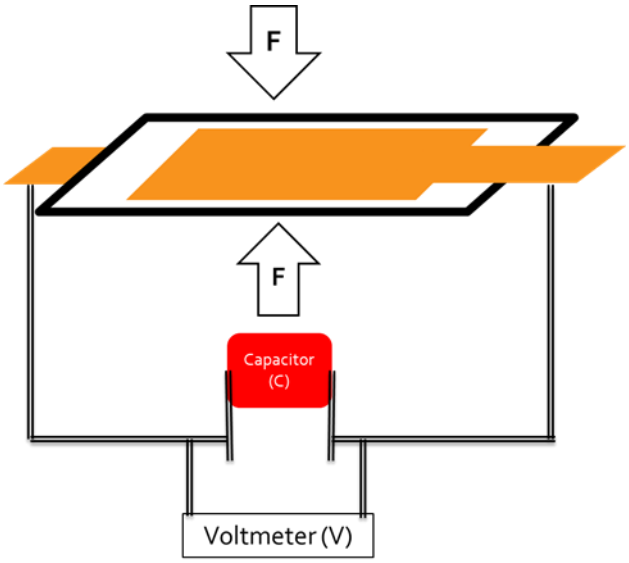

Figure 11. Modified Sawyer-Tower Circuit with PVDF sensor. The PVDF sensor shown as a black outlined square with orange copper tape electrodes is connected to the capacitor and the Voltmeter (V). The compressive forces are shown with the arrows labeled "F".

The PVDF sensors were placed on a 3D printed grip made of polylactic acid (PLA) and secured using scotch tape as shown in Figure 10. The sensor was connected to a modified Sawyer Tower circuit (Figure 11), in which the voltage generated from the PVDF sensor was collected across a 0.01uF capacitor. Each single voltage reading involved a multi-step process. In the first step, the tensile tester applied a preload of 8.90N (2lb$_f$) at a rate of 100mm/sec to the sample. The preload was held on the sample for 6 seconds, which was done to allow for the voltage to return to the baseline. The second step applied the actual compressive load to generate a voltage output, which was done by moving the upper grip 0.1mm, 0.2mm, 0.3mm, 0.4mm or 0.5mm downwards at a rate of 100mm/sec relative to the position of the grip after the preload was applied. This was done so that the load for each trial was approximately the same between replicates. Immediately after moving downward to the desired displacement, the grip returned to its home position, allowing the sample to relax and the voltage to return to its baseline. 5 replicates were performed at each displacement value, for a total of 25 trials per sample.

Since it was determined that thin-film piezoelectric materials cannot be used on a d_{33} meter since they are too thin and will not generate enough voltage, it was necessary to see the effects of stacking the PVDF sensors. Each weight percent ZnO PVDF sensor

membrane was subjected to compression tests in stacks of 1, 2, 3, and 4, and the voltage generated collected for comparison.

2.5 Data analysis methods

To calculate the d_{33} coefficient of the spongelike porous PVDF sensors, the following equation was used:

$$d_{33} = \frac{D}{\sigma} \tag{5}$$

where D is the electric displacement calculated by equation 6:

$$D = \frac{C*V}{A} \tag{6}$$

where C is the capacitance of the capacitor used in the Sawyer-Tower Circuit, V is the voltage generated from the sensor and A is the area of the electrode. σ is the stress applied to the sensor and is calculated using equation 7:

$$\sigma = \frac{F}{A} \tag{7}$$

where F is the force applied to the PVDF sensor and A is the area of the applied force. Since the area of the electrode and the area of the applied force is the same, the d_{33} coefficient can be calculated by combining equations 6 and 7:

$$d_{33} = \frac{C*V}{F} \tag{8}$$

which is reported in units of $\frac{pC}{N}$ (picocoulombs per Newton).

From each compression test, LabVIEW collected the voltage generated from the PVDF sensor (in V), the position of the grip (mm), and the load applied to the sensor (lb_f). Figure 12 shows a sample compression test result of a PVDF sensor. To calculate the voltage generated from the compression, first a baseline voltage was calculated. This was done by taking the maximum and minimum voltage from 0-1 seconds and dividing by 2 shown by the yellow arrow. In this specific trial, the preload can be seen from the change in voltage around the 2-second mark. The voltage then returns back to the baseline value. The maximum change in voltage was found when the load was applied to

the sensor. In this specific trial, the load is applied at around the 10-second mark indicated by the large change in the load, shown in orange, and the peak voltage is indicated by the green arrow. For this compression test, the large change in voltage was due to the release of the grip. The initial little change in voltage right before the 10-second mark is from the compression.

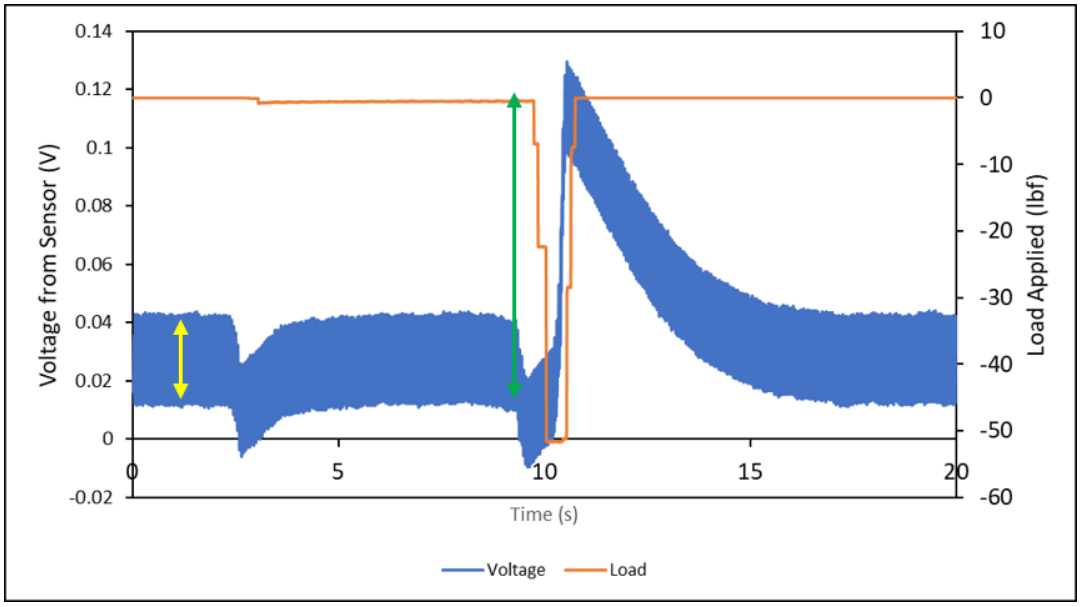

Figure 12. Sample compression test of a 30%wt ZnO sample subjected to a 0.5mm compression test in a stack of two. The baseline is calculated by adding the maximum and minimum noise values (denoted by the yellow arrow) and dividing by two. The peak voltage was the maximum change from the baseline, shown by the green arrow.

The maximum change in voltage and the magnitude of the load applied was then plotted with the other voltages and loads at different displacements. This can be seen in Figure 13 below.

Figure 13 shows an example of a linear regression of the voltages and the loads applied to a 30% wt ZnO PVDF sensor. This slope, which is equivalent to *V/F*, is used in the calculation of the d_{33} value. Multiplying the slope by the capacitance of the capacitor used in the circuit gives the d_{33} coefficient based on equation 8.

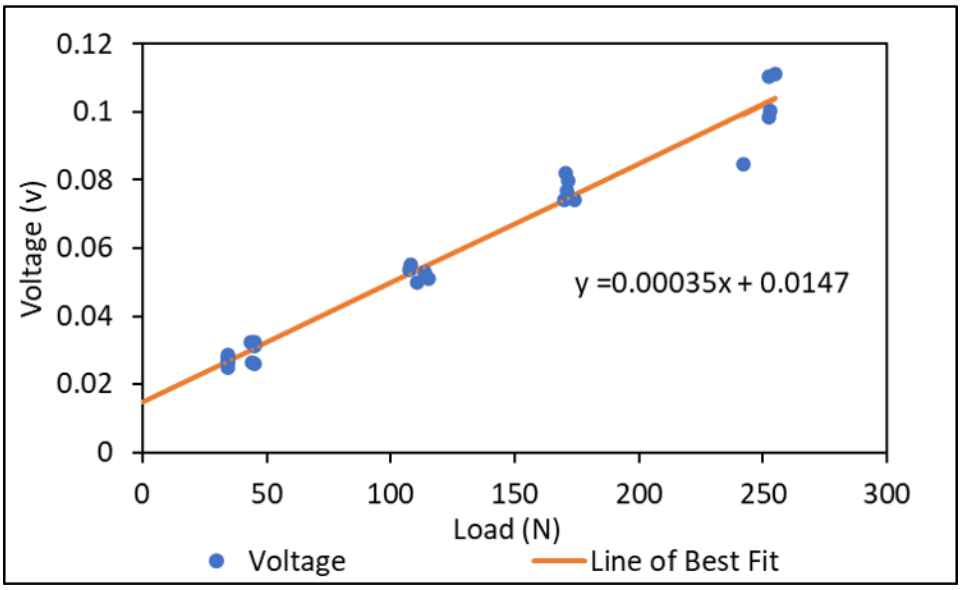

Figure 13. Linear regression of voltage vs load applied to a 30%wt ZnO PVDF sensor. The slope and intercept are noted on the plot.

Chapter 3. Results

3.1 Structural Results

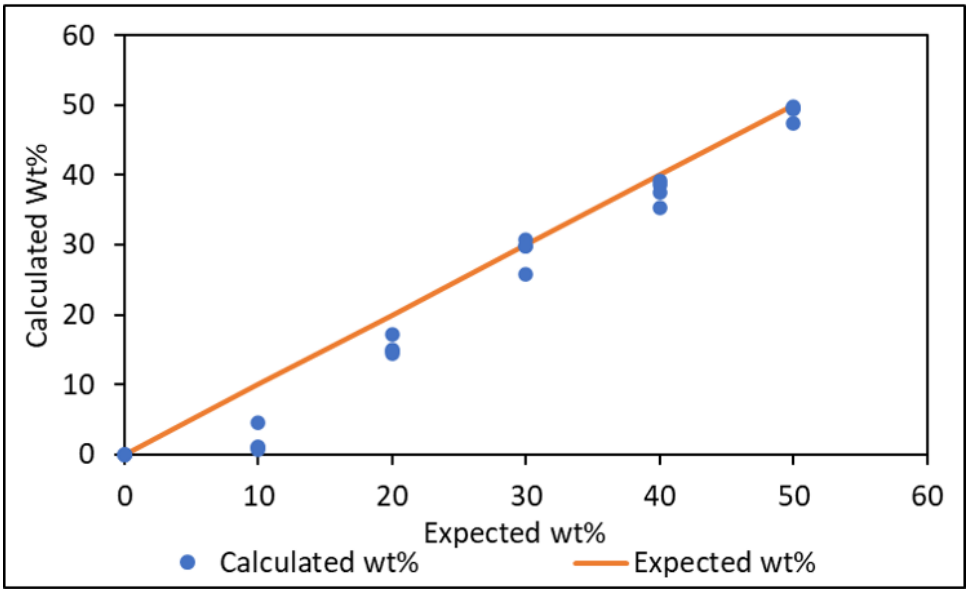

Figure 14. Calculated wt% vs Expected wt% of Porous PVDF sensors. The blue dots indicated the calculated wt% ZnO values and the orange line shows where the calculated wt% values would equal the Expected wt%.

During the fabrication process, the samples were weighed before the PVDF sensors were placed in the HCl acid bath. After spending 24h in the bath, the PVDF sensors were removed, dried, and re-weighed. This allowed for calculation of the wt% ZnO removed in the bath. Figure 14 shows the calculated wt% vs the expected wt%. The orange line designates full removal of the ZnO nanoparticles when the calculated wt% is equal to the expected wt%. The 10%wt ZnO and 20%wt ZnO had a higher mass than expected, which means not all the ZnO was removed, and the calculated wt% falls below the orange line. This is possibly due to the nanoparticles being trapped inside the PVDF sensor and the HCl is unable to penetrate the PVDF membrane and react with the ZnO. At a higher wt% ZnO, the HCl can dissolve more nanoparticles since the structure is more porous.

Figure 15A shows the porosities of the different wt% ZnO PVDF sensors from the gravimetric method, with Figure 12B showing the p-values from statistical comparisons using the One-Way ANOVA function in Origin (OriginLab Corporation,

A

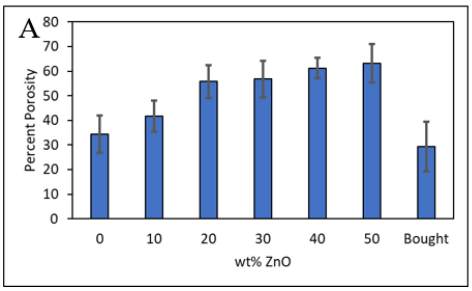

B

Wt% ZnO	Porosity	Std. Dev.	p-Value comparisons					
			10%	20%	30%	40%	50%	Bought
0	34.39	7.68	3.93E-01	5.63E-06	2.07E-06	1.16E-07	8.75E-08	9.02E-01
10	41.69	6.36		4.39E-03	1.76E-03	3.05E-05	5.01E-06	8.72E-02
20	55.78	6.72			1.00E+00	7.11E-01	3.73E-01	4.59E-06
30	56.84	7.41				8.69E-01	5.59E-01	2.03E-06
40	61.28	4.16					9.98E-01	1.51E-07
50	63.20	7.84						9.97E-08
Bought	29.32	10.18						

Figure 15. Percent Porosity of Fabricated and Bought PVDF sensors. n=8 for fabricated PVDF sensors and n=4 for bought PVDF samples. P-Value comparisons highlighted in green are significant at p<0.05.

Northampton, MA) with the Tukey post-hoc means comparison analysis. Both the plot and table of porosities and the p-level comparisons show two different groups of porosities. The 0% and 10%wt ZnO sensors as well as the bought samples had similar porosities and are not statistically different from each other. The porosities for the 20 through 50%wt ZnO sensors are similar and are not statistically different from each other as well. Each sensor in a group is statistically different from sensors from the other group at the 0.05 level. This suggests that adding ZnO nanoparticles to the PVDF sensors during the fabrication process does alter the porosity. Figure 14 shows that the calculated wt% for the 10%wt ZnO sensors were close to zero. This means the porosity of the 10%wt sensors should have similar porosity fractions as the 0%wt ZnO and bought samples, which is shown in Figure 15.

The gravimetric method shows that there is some porosity in the 0% wt ZnO without adding ZnO nanoparticles during the fabrication process. This suggests that PVDF samples are naturally porous to an extent. As expected, there is also a trend of increasing porosity with the increase in wt% ZnO during fabrication. This shows that the fabrication method is successful in creating sensors of varying porosities.

The final method to characterizing the structure of the PVDF sensors was using FTIR to find the relative amounts of each chain conformation present in the samples. Figure 16 shows the fraction of β *and* γ phases present in each PVDF sensor at various wt% ZnO and also includes the "bought" PVDF samples.

From Figure 16A, the bought PVDF samples were comprised of about a 73% fraction of *β and γ* phases, where all the fabricated samples had a fraction of 27% to 36%, which is significantly lower. Figure 136 lists the values of the fractions of *β and γ* phases as well as the p-values for all the comparisons. All the comparisons between the bought samples and the fabricated sensors were significant at the 0.05 level, which means the fabrication process between the bought samples and porous sensors are different and have an effect on chain conformation. Some of the fabricated sensors are statistically different from each other, such as 0%wt ZnO and the 30%wt ZnO sensors. This suggests that varying the ZnO nanoparticle concentration during the fabrication process has an effect on the chain conformation. Since there is no pattern or trend with wt% ZnO and chain conformation percent, this cannot be controlled via these current methods.

A

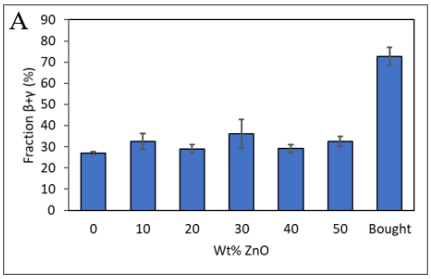

B

Wt%	Fraction β + γ	Std. Dev.	p-Value comparisons					
			10	20	30	40	50	Bought
0	27.05	0.75	7.82E-04	7.82E-01	2.13E-08	6.46E-01	6.61E-04	0
10	32.52	3.67		7.47E-02	8.89E-02	1.28E-01	1.00E+00	0
20	28.88	2.05			3.09E-06	1.00E+00	6.67E-02	0
30	36.07	6.75				8.20E-06	9.92E-02	0
40	29.16	1.91					1.16E-01	0
50	32.57	2.36						0
Bought	72.68	4.27						

Figure 16. Chain conformations of PVDF Polymer. The fraction of β and γ chain conformations in the PVDF sensors is shown above in A. The "Bought" PVDF had the largest fraction at 72.6%, which is double the highest of the fabricated PVDF sensors which was 30%Wt ZnO. n=16 for each type of sample. The p-value comparisons are shown in B. The green highlights significance at p<0.05.

3.2 Mechanical Results

Since very little voltage could be collected in a single stack for the fabricated PVDF, and the bought PVDF had a very low d_{33} value that was not close to the reported d_{33} value of 20pC/N[28], it was decided that the PVDF sensors need to be tested in at least stacks of 2. This result was expected since literature had noted that measuring thin piezoelectric materials does not give expected d_{33} values on the d_{33} meter[26,27].

Figure 17 shows all the d_{33} values for each wt% ZnO in the various stack sizes with Figures 17B, D, and F zooming in on 2,3, and 4 stacks respectively. Overall, the largest d_{33} value was found from the 30%wt ZnO sensors in a stack of 2. In stacks of 2, the d_{33} value increased from 0%wt up to 30%wt, and then the d_{33} value decreased as the wt% increased to 50%. There were no comparisons of d_{33} values that were statistically significant at the 0.05 level. Regardless, the shape of the change in d_{33} values with the

change in induced porosity during fabrication follows the hypothesis that porosity affects the piezoelectric output and that there is an optimal porosity for piezoelectric properties[19]. Figure 17D shows that having a stack of 3 PVDF sensors does alter the d_{33} coefficient but no comparisons were statistically significant like in stacks of 2. In stacks of 3, the 50%wt ZnO sensors had the largest piezoelectric effect. For stacks of 4 PVDF sensors, 30% wt ZnO had the highest d_{33} coefficient which is shown in Figure 17F and 17G. The d_{33} value for 30% wt ZnO was statistically different from the 0%wt and 40%wt ZnO sensors, as well as the 0%wt ZnO sensor statistically different from the 50%wt ZnO sample. Overall, Figure 17 shows that there is a dependence on porosity on the piezoelectric properties of fabricated PVDF sensors, although their large deviations render many comparisons insignificant. This could be due to changes in how aligned the stacks are between replicates. It is possible that the sensors were not perfectly aligned as well as air gaps present between sensors in the stacks. This would affect the orientation and possible alignment of PVDF chain conformations and change the piezoelectric output of the stacks.

A

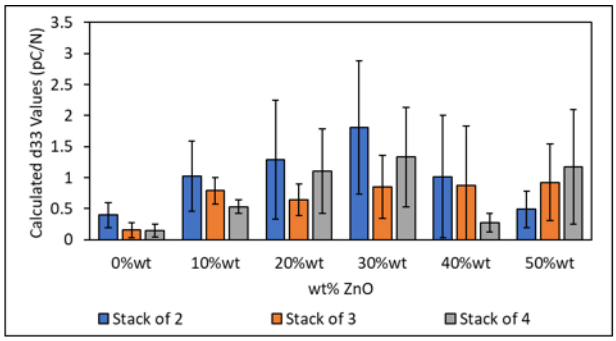

B

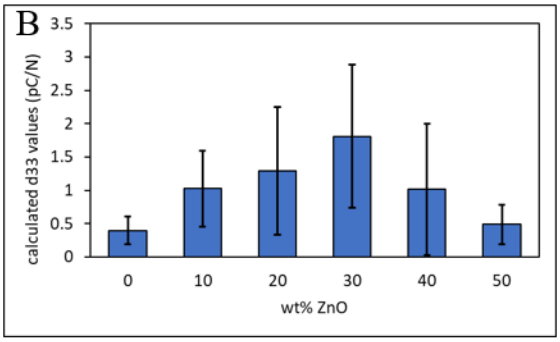

C

Wt% ZnO	d_{33} (pC/N)	Std. Dev.	p-Value comparisons				
			10	20	30	40	50
0	0.40	0.21	9.84E-01	9.16E-01	5.76E-01	9.88E-01	1.00E+00
10	1.02	0.57		1.00E+00	9.23E-01	1.00E+00	9.88E-01
20	1.29	0.96			9.90E-01	1.00E+00	9.14E-01
30	1.81	1.07				9.34E-01	5.25E-01
40	1.02	0.99					9.91E-01
50	0.49	0.29					

D

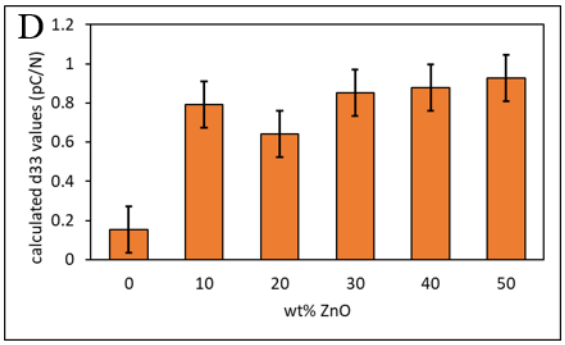

E

Wt% ZnO	d_{33} (pC/N)	Std. Dev.	p-Value comparisons				
			10	20	30	40	50
0	0.15	0.12	4.69E-01	7.29E-01	3.71E-01	3.31E-01	3.05E-01
10	0.79	0.22		9.97E-01	1.00E+00	1.00E+00	9.98E-01
20	0.64	0.25			9.84E-01	9.73E-01	9.51E-01
30	0.85	0.50				1.00E+00	1.00E+00
40	0.88	0.96					1.00E+00
50	0.93	0.61					

F

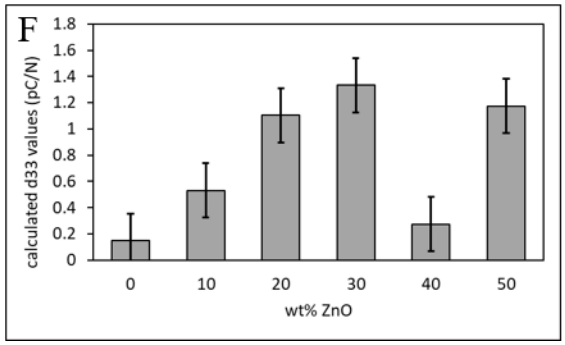

G

Wt% ZnO	d_{33} (pC/N)	Std. Dev.	p-Value comparisons				
			10	20	30	40	50
0	0.15	0.11	8.56E-01	7.39E-02	1.47E-02	9.99E-01	4.64E-02
10	0.53	0.11		6.92E-02	1.87E-01	9.70E-01	4.08E-01
20	1.10	0.68			9.82E-01	1.59E-01	1.00E+00
30	1.33	0.80				3.67E-02	9.97E-01
40	0.27	0.15					1.05E-01
50	1.17	0.92					

Figure 17. d_{33} values for fabricated PVDF sensors in stacks of 2, 3 and 4. A shows the d_{33} values by wt% ZnO and by stack size. B shows d_{33} values for stacks of 2, and C shows the p-value comparisons for stacks of 2. D shows the d_{33} values in stacks of 3, E shows the p-value comparisons for the stacks of 3. F shows the d_{33} values in stacks of 4 with the p-value comparisons in G. Green highlights significance at $p<0.05$. $n=3$ through $n=6$ for the number of replicates at each stack size at each wt% ZnO.

Figure 18A and Figure 18B show the d_{33} values of different stack sizes of the bought PVDF. The single stack of bought PVDF had the lowest d_{33} value and the stack of 3 had the highest d_{33} value. Since the p-value comparing the stack of 1 with stacks of 3 and 4 are statistically different at $p<0.05$, this suggests that stacking the bought PVDF samples influences the d_{33} values. This supports the need to stack PVDF samples to get a more accurate reading of thin-film piezoelectric materials to calculate the d_{33} values. The d_{33} values for the bought PVDF were about an order of magnitude larger than the fabricated PVDF sensors. The largest d_{33} value for the purchased PVDF was 13.3pC/N, while the largest fabricated value was 1.8pC/N.

Figure 19 shows the d_{33} coefficients of each wt% ZnO compared to the fraction of β and γ chain conformations present in the samples in a stack of 2. This chart shows that as the fraction of β and γ chain conformations present increased, the piezoelectric output of the samples also increased. This result confirms that the piezoelectric properties of PVDF are dependent on the amount of β and γ chain phases, which are the phases that exhibit piezoelectric properties.

A

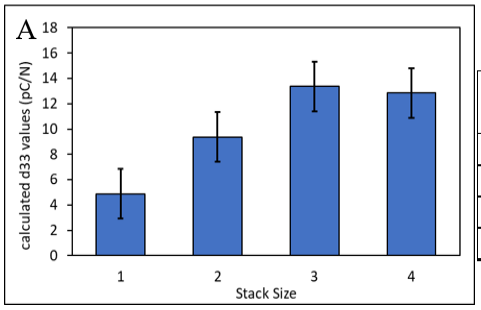

B

Stack Size	d_{33} (pC/N)	Std. Dev.	p-Value comparisons		
			2	3	4
1	4.88	0.75	2.64E-01	2.25E-02	3.06E-02
2	9.37	3.72		3.49E-01	4.52E-01
3	13.35	0.96			9.96E-01
4	12.85	3.85			

Figure 178. d_{33} for bought PVDF in stacks of 1, 2, 3 and 4. B shows the p-value comparisons between each stack. Green highlights significance at $p<0.05$.

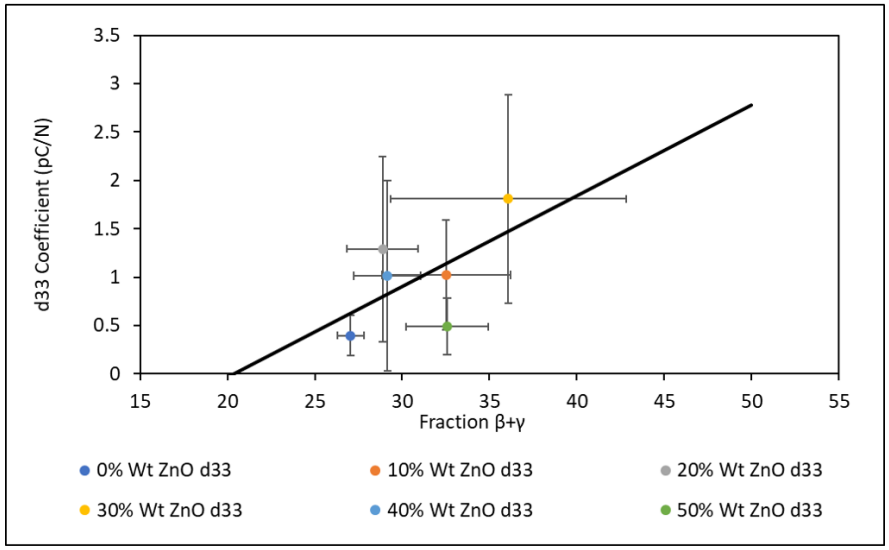

Figure 19. d_{33} values of 2 stacks of fabricated PVDF sensors compared to fraction of β and γ chain conformations. The black line indicates a trendline of increasing d_{33} values with increasing of β and γ chain conformations. The error bars show the standard deviation of the d_{33} values, and the standard deviation of chain conformations.

Chapter 4. Discussion and Future Work

4.1 Discussion of Results

The results from this study show adding ZnO nanoparticles to the dissolved PVDF solution can induce additional pores to the sensor. Varying the wt% ZnO also altered the chain conformations of the polymer as shown by the FTIR structural characterization. Finally, the various concentrations of ZnO added during the fabrication process had effects on the d_{33} coefficients of PVDF.

The porosity test gave results that were expected, in that adding ZnO nanoparticles during the fabrication process (and subsequently removing them in the HCl bath) increased the porosity of the PVDF sensors. Since the bought samples had a porosity around 29% volume and the 0%Wt ZnO had a porosity of about 34%, and they were not statistically different, it can be assumed that the bought PVDF was fabricated without the introduction of additional pores. The bought PVDF and the 0%wt ZnO senors are similar in porosity. Since both the bought and the 0%wt ZnO samples had some pores, PVDF must naturally form a structure that has some pores. This makes sense since in the biochemistry field, PVDF is used in western blots, which are used to detect different-sized proteins by filtering them through a porous PVDF membrane [29]. This porous phenomenon is also observed in other thin film polymers for use in separation and purification applications, tissue engineering, semiconductor devices and energy applications [30–34]. For example, Akolekar et al noted that the polymers used for purification had porous properties without inducing pores during the fabrication process[31].

The FTIR results show that the amount of β and γ phases present in the PVDF sensors are dependent on the amount of ZnO added due to different conformation fractions being statistically different from each other (when $p<0.05$). This means that adding different amounts of ZnO to the dissolved PVDF solution during the fabrication process not only alters the porosity but also alters the polymer chain conformation during the evaporation process. Since there does not seem to be a trendline of fraction β and γ phases and amount ZnO added, the fraction of fraction β and γ phases cannot be controlled or altered intentionally. When adding ZnO nanoparticles during the fabrication

process, the goal was to alter the porosity of the samples, not change the amount of β and γ phases present in the sensor. The porosity and FTIR results suggest that changing the amount of ZnO nanoparticles introduces two confounding factors that both alter the piezoelectric properties: increasing the porosity not only allows larger deformations to the PVDF chains which would generate a larger piezoelectric output, but also alters the amount of polarized β and γ phases.

The bought PVDF had a 72% fraction of β and γ phases present in the sample, which is much higher than all of the fabricated nanoporous samples in this study. This is probably due to a process called poling. Poling applies a large electric field to a sample to alter different chain conformations in PVDF. The fabricated PVDF samples were not poled for this project. Since the bought samples were poled, they are considered polarized and have a positively oriented side and a negatively oriented side. This means the electric field forced the bonds between carbon atoms to a trans configuration rather than alternating between trans and gauche. This would make the PVDF have a higher amount of β *and* γ phases present, which is supported by Figure 16 showing the fraction of β *and* γ phases present at a high level of 70%. Poling the PVDF sensors after the fabrication process should hypothetically increase the fraction β *and* γ phases in the sensors since literature shows that poling changes the chain conformation of PVDF [35].

Instead of poling PVDF, the effects of porosity were the focus of this study. The calculated d_{33} values from the compression tests show that there is an optimal porosity for maximizing the piezoelectric output. This is supported by looking at the stacks of two films and four films. The 30% wt ZnO sensor had the largest d_{33} value, and this can be partially attributed to the addition of induced pores. It is thought that introducing pores allows the PVDF to deform, or flex, more[19]. This increases the polarization of the PVDF polymer chain and increases its piezoelectric output while having less PVDF present in the sample. Specifically, the stacks of two data shows an increase of d_{33} coefficients up to 30%, and then a decrease in piezoelectric output as porosity increases. The pattern of peak piezoelectric properties at 30%wt ZnO show a tradeoff of removing PVDF from the sensor. Removing some PVDF improves the piezoelectric properties to an extent, removing too much results in lower d_{33} values showing an optimal ZnO composition.

This supports the hypothesis that porosity has an effect on piezoelectric output and these results are supported by literature[19,20]. The d_{33} coefficient also follows a pattern with the highest fraction β *and* γ phases peaking at the 30%wt ZnO. Since the d_{33} increased with both porosity and fraction β *and* γ phases (which cannot be controlled), the piezoelectric properties depend on both factors.

Stacking the samples allowed for voltage measurements for calculating the d_{33} coefficient, but ideally, minimizing the stack size is the goal. Literature shows that thin-film piezoelectric materials may not exhibit expected piezoelectric properties while being tested since they are very thin and especially if they are "soft" materials [27]. Thin piezoelectric materials had a lower mean d_{33} coefficient compared to thicker samples of the same material [27]. This can be partly attributed to the geometry of the piezoelectric material, if the stacked samples are not perfectly aligned, this could lower the polarization of the material and lower the piezoelectric properties. This can be seen in the above data since the d_{33} values decreased for most Wt% ZnO as the number of sensors in a stack increased. One issue with stacking sensors is that if the samples are polarized, like the bought PVDF, there is a possibility that the orientation of the samples would not be perfectly aligned, which would lower the piezoelectric effect and produce a smaller voltage.

These fabricated sensors, as of right now, would not work for our purpose to detect changes in blood flow and blood pressure. Normal blood pressure is around 120mmHg systolic and 80mmHg diastolic [36], which is 10.3 N/in^2 and 6.88 N/in^2 respectively. This means the PVDF sensors will be subjected to forces between 10.3 and 6.88N, based on a reasonable sensor square of 1"x1". Unfortunately, at this point, the sensor generates a noise level around 0.02V when not compressed, and using the slope for the optimal sensor, we would not detect a change. There are some options to increase the sensitivity of the PVDF sensors. Since the bought PVDF samples were similar to the 0%wt ZnO in terms of porosity but different in β and γ phases, poling could theoretically increase the β and γ chain conformations. This should increase the d_{33} coefficient in the 0%Wt ZnO samples. If increasing the fraction of β *and* γ chains present increases the

piezoelectric output of 0%Wt ZnO, it could also mean that the porous PVDF sensors could have a higher d_{33} coefficient as well.

4.2 Future Work

Going forward, the fabrication process will need modification to improve the d_{33} values of the porous PVDF sensors. Investigation of methods that alter the fraction of β and γ phases present in the sensors is needed. This could be done by applying a large electric field to the sensors through the poling process. Fabricating sensors that don't require stacking to collect the d_{33} value would be ideal. This could be possibly solved by casting a larger volume of PVDF/ZnO solution or fusing two different sensors together. Other studies on PVDF sensors have found that having larger amounts of PVDF in the sample lead to larger piezoelectric properties, which could be investigated further for these sensors by altering the composition of starting materials[37].

Bibliography

(1) Transcatheter aortic valve replacement (TAVR) - Mayo Clinic https://www.mayoclinic.org/tests-procedures/transcatheter-aortic-valve-replacement/about/pac-20384698 (accessed 2021 -06 -22).

(2) Aortic Stenosis Overview https://www.heart.org/en/health-topics/heart-valve-problems-and-disease/heart-valve-problems-and-causes/problem-aortic-valve-stenosis (accessed 2021 -08 -05).

(3) Culler, S. D.; Cohen, D. J.; Brown, P. P.; Kugelmass, A. D.; Reynolds, M. R.; Ambrose, K.; Schlosser, M. L.; Simon, A. W.; Katz, M. R. Trends in Aortic Valve Replacement Procedures Between 2009 and 2015: Has Transcatheter Aortic Valve Replacement Made a Difference? *The Annals of Thoracic Surgery* **2018**, *105* (4), 1137–1143. https://doi.org/10.1016/j.athoracsur.2017.10.057.

(4) TAVR vs SAVR: Comparing Transcatheter & Surgical Aortic Valve Replacement https://healthblog.uofmhealth.org/heart-health/tavr-vs-savr (accessed 2021 -07 -19).

(5) Mazzella, A. J.; Hendrickson, M. J.; Arora, S.; Sanders, M.; Li, Q.; Vavalle, J. P.; Gehi, A. K. Shifting Trends in Timing of Pacemaker Implantation After Transcatheter Aortic Valve Replacement. *JACC: Cardiovascular Interventions* **2021**, *14* (2), 232–234. https://doi.org/10.1016/j.jcin.2020.09.034.

(6) Valverde, I.; Gomez, G.; Coserria, J. F.; Suarez-Mejias, C.; Uribe, S.; Sotelo, J.; Velasco, M. N.; Soto, J. S. D.; Hosseinpour, A.-R.; Gomez-Cia, T. 3D Printed Models for Planning Endovascular Stenting in Transverse Aortic Arch Hypoplasia. *Catheterization and Cardiovascular Interventions* **2015**, *85* (6), 1006–1012. https://doi.org/10.1002/ccd.25810.

(7) Thorburn, C.; Abdel-Razek, O.; Fagan, S.; Pearce, N.; Furey, M.; Harris, S.; Bartellas, M.; Adams, C. Three-Dimensional Printing for Assessment of Paravalvular Leak in Transcatheter Aortic Valve Implantation. *J Cardiothorac Surg* **2020**, *15*, 211. https://doi.org/10.1186/s13019-020-01255-3.

(8) Jo M. Zelis; Meiburg, R.; Jorn Roijen; Koen Janssens; Marcel Veer; Nico Pijls; Nils Johnson; Frans de Vosse; Pim Tonino; Marcel Rutten. 3D-Printed Stenotic Aortic Valve Model to Simulate Physiology before, during, and after Transcatheter Aortic Valve Implantation | Elsevier Enhanced Reader. *International Journal of Cardiology 313* (2020), 32–34. https://doi.org/10.1016/j.ijcard.2020.04.087.

(9) Tanimoto, M.; Arai, F.; Fukuda, T.; Iwata, H.; Itoigawa, K.; Gotoh, Y.; Hashimoto, M.; Negoro, M. Micro Force Sensor for Intravascular Neurosurgery and in Vivo Experiment. In *Proceedings MEMS 98. IEEE. Eleventh Annual International Workshop on Micro Electro Mechanical Systems. An Investigation of Micro Structures, Sensors, Actuators, Machines and Systems (Cat. No.98CH36176*; 1998; pp 504–509. https://doi.org/10.1109/MEMSYS.1998.659809.

(10) Tressler, J. F.; Alkoy, S.; Newnham, R. E. Piezoelectric Sensors and Sensor Materials. 16.

(11) Yen-Fang Su; Guangshuai Han; Zhihao Kong; Tommy Nantung; Na Lu. Embeddable Piezoelectric Sensors for Strength Gain Monitoring of Cementitious

Materials: The Influence of Coating Materials. *Engineered Science* **2020**, *2020* (11), 66–75.
(12) Baptista, F. G.; Budoya, D. E.; Almeida, V. A. D. de; Ulson, J. A. C. An Experimental Study on the Effect of Temperature on Piezoelectric Sensors for Impedance-Based Structural Health Monitoring. *Sensors* **2014**, *14* (1), 1208–1227. https://doi.org/10.3390/s140101208.
(13) Cai, X.; Lei, T.; Sun, D.; Lin, L. A Critical Analysis of the α, β and γ Phases in Poly(Vinylidene Fluoride) Using FTIR. *RSC Adv.* **2017**, *7* (25), 15382–15389. https://doi.org/10.1039/C7RA01267E.
(14) Ruan, L.; Yao, X.; Chang, Y.; Zhou, L.; Qin, G.; Zhang, X. Properties and Applications of the β Phase Poly(Vinylidene Fluoride). *Polymers* **2018**, *10* (3), 228. https://doi.org/10.3390/polym10030228.
(15) Wan, C.; Bowen, C. R. Multiscale-Structuring of Polyvinylidene Fluoride for Energy Harvesting: The Impact of Molecular-, Micro- and Macro-Structure. *J. Mater. Chem. A* **2017**, *5* (7), 3091–3128. https://doi.org/10.1039/C6TA09590A.
(16) Li, Q.; Xing, J.; Shang, D.; Wang, Y. A Flow Velocity Measurement Method Based on a PVDF Piezoelectric Sensor. *Sensors* **2019**, *19* (7), 1657. https://doi.org/10.3390/s19071657.
(17) McLaughlin, J.; McNeill, M.; Braun, B.; McCormack, P. D. Piezoelectric Sensor Determination of Arterial Pulse Wave Velocity. *Physiol. Meas.* **2003**, *24* (3), 693–702. https://doi.org/10.1088/0967-3334/24/3/306.
(18) Takashima, K.; Horie, S.; Mukai, T.; Ishida, K.; Matsushige, K. Piezoelectric Properties of Vinylidene Fluoride Oligomer for Use in Medical Tactile Sensor Applications. *Sensors and Actuators A: Physical* **2008**, *144* (1), 90–96. https://doi.org/10.1016/j.sna.2008.01.015.
(19) Mao, Y.; Zhao, P.; McConohy, G.; Yang, H.; Tong, Y.; Wang, X. Sponge-Like Piezoelectric Polymer Films for Scalable and Integratable Nanogenerators and Self-Powered Electronic Systems. *Adv. Energy Mater.* **2014**, *4* (7), 1301624. https://doi.org/10.1002/aenm.201301624.
(20) Yan Zhang; Chris R. Bowen; Sylvain Deville. Ice-Templated Poly(Vinylidene Fluoride) Ferroelectrets. *Soft Matter 2019* (15), 825–832. https://doi.org/10.1039/c8sm02160k.
(21) Ramin Roshani; Fatemeh Ardeshir; Peyravi, M.; Mohsen Jahanshahi. Highly Permeable PVDF Membrane with PS/ZnO Nanocomposite Incorporated for Distillation Process. *Royal Society of Chemistry* **2018**, *2018* (8), 23499–23515. https://doi.org/10.1039/c8ra02908c.
(22) A. Salimi; A.A. Yousefi. FTIR Studies of β-Phase Crystal Formation in Stretched PVDF Films. *Polymer Testing 2003* (22), 699–704.
(23) Masamichi Kobayashi; Tashiro, K.; Hiroyuki Tadokoro. Molecular Vibrations of Three Crystal Forms of Polyvinylidene Fluoride. *Macromolecules* **1974**, *8* (2), 158–170.
(24) Barrau, S.; Ferri, A.; Da Costa, A.; Defebvin, J.; Leroy, S.; Desfeux, R.; Lefebvre, J.-M. Nanoscale Investigations of α- and γ-Crystal Phases in PVDF-Based Nanocomposites. *ACS Appl. Mater. Interfaces* **2018**, *10* (15), 13092–13099. https://doi.org/10.1021/acsami.8b02172.

(25) Chen, W.; An, Z.; He, L.; Deng, Z. Piezoelectric Coefficients Measurement for PVDF Films with Pneumatic Pressure Rig in a Sole Cavity. In *2015 Symposium on Piezoelectricity, Acoustic Waves, and Device Applications (SPAWDA)*; IEEE: Jinan, China, 2015; pp 111–114. https://doi.org/10.1109/SPAWDA.2015.7364452.
(26) Huang, Z.; Zhang, Q.; Corkovic, S.; Dorey, R.; Whatmore, R. W. Comparative Measurements of Piezoelectric Coefficient of PZT Films by Berlincourt, Interferometer, and Vibrometer Methods. *IEEE Transactions on Ultrasonics, Ferroelectrics, and Frequency Control* **2006**, *53* (12), 2287–2293. https://doi.org/10.1109/TUFFC.2006.175.
(27) Stewart, M.; Battrick, W.; Cain, M. Good Practice Guide. 34.
(28) PVDF piezoelectric film, 28um/45um/120 um thick, Thick Screen-Printed Silver Electrode, energy harvesting, piezo sensor https://piezopvdf.com/pvdf-piezoelectric-film-thick-silver-ink/ (accessed 2021 -08 -18).
(29) Membranes and Filter Papers for Western Blotting | Thermo Fisher Scientific - US https://www.thermofisher.com/us/en/home/life-science/protein-biology/protein-assays-analysis/western-blotting/transfer-proteins-western-blot/membranes-transfer-buffers-western-blotting.html (accessed 2021 -08 -16).
(30) Hedrick, J. L.; Miller, R. D.; Hawker, C. J.; Carter, K. R.; Volksen, W.; Yoon, D. Y.; Trollsås, M. Templating Nanoporosity in Thin-Film Dielectric Insulators. *Advanced Materials* **1998**, *10* (13), 1049–1053. https://doi.org/10.1002/(SICI)1521-4095(199809)10:13<1049::AID-ADMA1049>3.0.CO;2-F.
(31) D. B. Akolekar; A. R. Hind; S. K. Bhargava. Synthesis of Macro-, Meso-, and Microporous Carbons from Natural and Synthetic Sources, and Their Application as Adsorbents for the Removal of Quaternary Ammonium Compounds from Aqueous Solution. *journal of Colloid and Interface Science* **1997**, *199*, 92–98.
(32) Lewandowski, K.; Murer, P.; Svec, F.; Fréchet, J. M. J. The Design of Chiral Separation Media Using Monodisperse Functionalized Macroporous Beads: Effects of Polymer Matrix, Tether, and Linkage Chemistry. *Anal. Chem.* **1998**, *70* (8), 1629–1638. https://doi.org/10.1021/ac971196x.
(33) Hubbell, J. A. Biomaterials in Tissue Engineering. 12.
(34) Vilela, F.; Zhang, K.; Antonietti, M. Conjugated Porous Polymers for Energy Applications. *Energy Environ. Sci.* **2012**, *5* (7), 7819. https://doi.org/10.1039/c2ee22002d.
(35) Hartono, A.; Darwin; Ramli; Satira, S.; Djamal, M.; Herman. Electric Field Poling 2G V/m to Improve Piezoelectricity of PVDF Thin Film; Bali, Indonesia, 2016; p 030021. https://doi.org/10.1063/1.4943716.
(36) Understanding blood pressure: What is normal? https://www.medicalnewstoday.com/articles/270644 (accessed 2021 -08 -15).
(37) Jared Tucker; Matthew Danley; Jack Kloster; Ping Zhao; Victor Lai. Effect of Fabrication Conditions on the Performance of Porous Polyvinylidene Fluoride (PVDF) Piezoelectric Sensors under Compression. *CRMC* **2021**, *1* (2021). https://doi.org/10.33790/crmc1100110.